INFRARED RADIATION FROM THE SPACE SHUTTLE CONTAMINANT ENVIRONMENT

J. P. Simpson* and F. C. Witteborn

Space Science Division

NASA Ames Research Center, Moffett Field, CA 94035

Abstract. The Space Shuttle contaminant environment consists of molecules and particles originating on the Shuttle. The molecules come from outgassing, cabin leakage, flash evaporators and other man-controlled vents, and rocket exhaust. Particles are thought to come from abrasion, ablation of surfaces, dust trapped in cracks, dust from vents and cabin leaks, ice particles from improper venting, and droplets of unburned fuel. Simpson and Witteborn (1977, Applied Optics 16, 2051-2073) have discussed the effect of the infrared radiation from molecules and particles from 4 μm to 200 μm on a sensitive infrared telescope. (This paper also discusses non-Shuttle infrared sources such as the atmosphere of the earth and the interplanetary dust/zodiacal light.) They conclude that the radiation from the contaminant environment is tolerable only when it is at its minimum, when there are no rocket firings and the flash evaporators and the manually controlled vents are not being used. This report extends the predicted infrared spectrum from the molecular contaminants H_2O and CO_2 down to 2 μm. It also discusses the sighting frequency and infrared spectrum of particles caused by spallation of the surfaces of the Shuttle tiles by micrometeoroid impact.

H_2O and CO_2 are the most important infrared active molecules that come from outgassing, cabin leakage, or evaporators. It is assumed that

---

*Ames Associate under Contract NAS2-9636.

the initial populations of the molecular levels are given by thermodynamic equilibrium (TE). In a vacuum the molecules radiate until they come into equilibrium with the radiation field of the earth and sun. The time it takes depends on the Einstein transition probability. Meanwhile the molecules move away from the Shuttle; only the nearby ones are detected by Shuttle-borne experiments. Consequently, the radiation from transitions with small transition probabilities (long lifetimes) is given by the TE formulae (such as the 15-μm band of CO_2 and the 6.3-μm band of H_2O). Bands with large transition probabilities (such as the 4.3-μm band of CO_2 and the 2.7-μm band of H_2O are in equilibrium with the radiation field of the sun or earth (the latter is very weak). Since the Shuttle is actually moving through the earth's upper atmosphere, the H_2O bands are also excited by collisions with oxygen atoms. This results in additional radiation. For CO_2 this excitation is almost negligible.

The surface of the Shuttle tiles is coated with borosilicate glass. Hypervelocity impacts of micrometeoroids make small craters, from which particles are ejected at high velocities (other particles are ejected at low velocities). The shocked or even melted particles have much higher temperatures than the surface; they cool to ambient within a few seconds. However, because of the high velocities, most of the particles that pass through the 15 arcmin field of view of a 1-m diameter telescope do so almost immediately after ejection. The spectrum of the 1 to 20-μm particles is that of a silicate, with emission peaks at 10 μm and 20 μm and emissivities that decrease rapidly at longer wavelengths.

Estimates of radiation from the sources discussed here do not change the authors' earlier conclusion that the Shuttle environment would be suitable for sensitive infrared astronomical observations with appropriate constraints on Shuttle observations. The nature of the expected sources, however, should be considered in the design of instruments planned for use in the Shuttle environment.

1. INTRODUCTION

The performance of cooled infrared telescopes observing from the Space Shuttle Orbiter will be limited by the background radiation from zodiacal particles and, to some extent, from the contaminant atmosphere of the Orbiter itself. Simpson and Witteborn[1] have estimated the infrared background in the 4 to 300 μm range for the expected contaminant environment. They found that with adequate operational constraints, the Orbiter can provide a suitable environment for a cooled infrared telescope. The evaluation was made using a molecular contaminant atmosphere determined by Rantanen and Ress[2] and design parameters from the Shuttle Infrared Telescope Facility (SIRTF), a 1.2-m diameter telescope with 10K - 20K optics.[3] The potential use of such an instrument on important problems which may have their solutions in the near infrared, coupled with the minimum in natural background near 3 μm, has brought to light the importance of evaluating the contaminant induced infrared background from 2 to 4 μm. This is done for water vapor and CO_2 considering both radiative and collisional effects at an altitude of 350 km.

While the particulate environment of the Shuttle Orbiter remains much less predictable than the molecular environment, a potentially important particle production mechanism, namely spallation by micrometeoroids incident upon the tiled surface of the Orbiter, has been proposed by Barengoltz.[4] The particle sighting rates resulting from this mechanism are examined here. The spectrum of the ejected particles is predicted for various sizes of particles of the composition of the tiles. The particle sighting rates determined for this mechanism may be high enough to require that the most sensitive SIRTF instruments incorporate particle sighting discrimination procedures or hardware. They are, however, discrete events and thus do not produce a continuously elevated background. The absence of a continuously elevated background due to spacecraft corona around Skylab was reported by Schuerman and Weinberg.[5]

We will discuss here the infrared spectrum of H_2O and CO_2 at fairly high resolution and the spectrum and sighting frequency of particles spalled by micrometeoroids. Units will be kept general so that the results can be applied to any instrument operating in that wavelength range.

2. MOLECULAR CONTAMINANTS

In this section we will discuss the infrared spectrum of molecular H_2O and CO_2 that is offgassed, outgassed, purposefully evaporated, or leaked from the Orbiter cabin. The temperature of the vapor is low, ranging from 201K for certain parts of the Shuttle facing cold space, to 366K for the radiators when they are facing the sun. We will consider

here only the temperature 296K because that is the temperature appropriate for cabin leakage. However, as will be seen, the molecules are not in equilibrium, and the radiation shortward of 5 μm does not depend on the initial temperature.

Bareiss et al.[6] have predicted column densities of H_2O and CO_2 for these sources. Column densities of H_2O for offgassing range from 10^{11} molecules/cm^2 for the minimum temperatures to greater than 10^{13} molecules/cm^2 for maximum temperatures and certain lines of sight. Column densities for the flash evaporators (when operating) range from a few times 10^{11} to a few times 10^{12} molecules/cm^2, depending on the line of sight. Both H_2O and CO_2 are leaked from the Orbiter cabin; the column densities are 1 to $5x10^{11}$ molecules/cm^2, depending on the line of sight. In addition the RCS Vernier thrusters produce the following infrared emitting contaminant molecules: CO, CO_2, H_2O, NO, and OH. The column densities range from 10^{12} to 10^{14} molecules/cm^2 depending on the thruster location. However, the temperature of the exhaust gas is so high that the infrared radiation from the gas is much more intense than that from any other source. Consequently, we will not consider the vernier thruster exhaust because it would not be worthwhile for sensitive infrared telescopes to take data while the thruster exhaust is in the field of view. The gaseous exhaust products dissipate in a few seconds so the lost observing time is negligible, provided that the interval between firings is large.

In this paper we will not consider the spectra of other molecules besides H_2O and CO_2. Such molecules might be the outgassed products of

epoxy, teflon, paint, insulation, etc. We will also assume there are no leaks in the fuel, hydraulic, and coolant systems. Finally, we will not consider the gases that might be leaked from or used to purge other experiments.

When the H_2O and CO_2 molecules leave the Shuttle, they move into the radiation field of the earth and sun. We assumed that all the molecules move with the most probable velocity for the temperature 296K. Rantanen and Ress[2] have predicted the density of the molecules as functions of distance from the Shuttle and line of sight. From this we can calculate the number of molecules in the line of sight that fall into each time increment. Half the column density is reached by 21.3 m for H_2O and by 13.1 m for CO_2; the corresponding travel times for the molecules are 0.041 sec and 0.039 sec, respectively. It was assumed that the instrument's entrance aperture projects 3 m beyond the skinline of the Orbiter. The radiation field of the sun is approximately a blackbody at 5850K diluted by the solid angle of the sun divided by 4 π ster. The radiation field of the earth is given by a blackbody function at different temperatures subtending 2 π ster. (The actual solid angle is slightly smaller and varies with altitude.) The different temperatures are the brightness temperatures of the earth at different wavelengths given by Smith.[7] The brightness temperature is as low as 218K where the earth's atmosphere is optically thick, but 288K where the atmosphere is optically thin and one can see all the way to the surface of the earth from space. Because of the short time required for the molecules to

disperse out of the field of view, the vibration-rotation bands could be divided into three groups. 1) Those with transition probabilities A greater than about 80 sec^{-1}, such as the 4.3-μm band of CO_2 and the 2.7-μm band of H_2O come into equilibrium almost immediately, as $(1-e^{-At})$. 2) Bands with A less than a few sec^{-1} do not substantially change their initial intensities in the few tenths of a second that it takes before they are dispersed out of the field of view. 3) Intermediate cases fall between. We did a molecular excitation and decay calculation for those vibrational levels from which bands in groups 1 and 3 arise. All vibration-rotation bands connecting these levels were considered. There were 7 vibrational levels in the calculation for H_2O and 11 for CO_2 (more because of the extra degeneracy in the linear CO_2). The initial populations of the rotational levels in each vibrational level were given by the Boltzmann equation for 296K. The level populations were then followed for 0.27 sec, at which time the column density has fallen to less than a tenth of the total value. The line list by McClatchey et al.[8] was used for the energy levels and transition probabilities. The spectrum at each increment of 0.01 sec was multiplied by the fraction of the column density in that time increment and summed. All transitions not included in this calculation (all of group 2) were added with their initial small intensities.

The spectrum for a column density of 10^{12} molecules/cm^2 of H_2O is given in Fig. 1, and the spectrum for 10^{11} molecules/cm^2 of CO_2 is given in Fig. 2. These are probably close to the minimum column densities

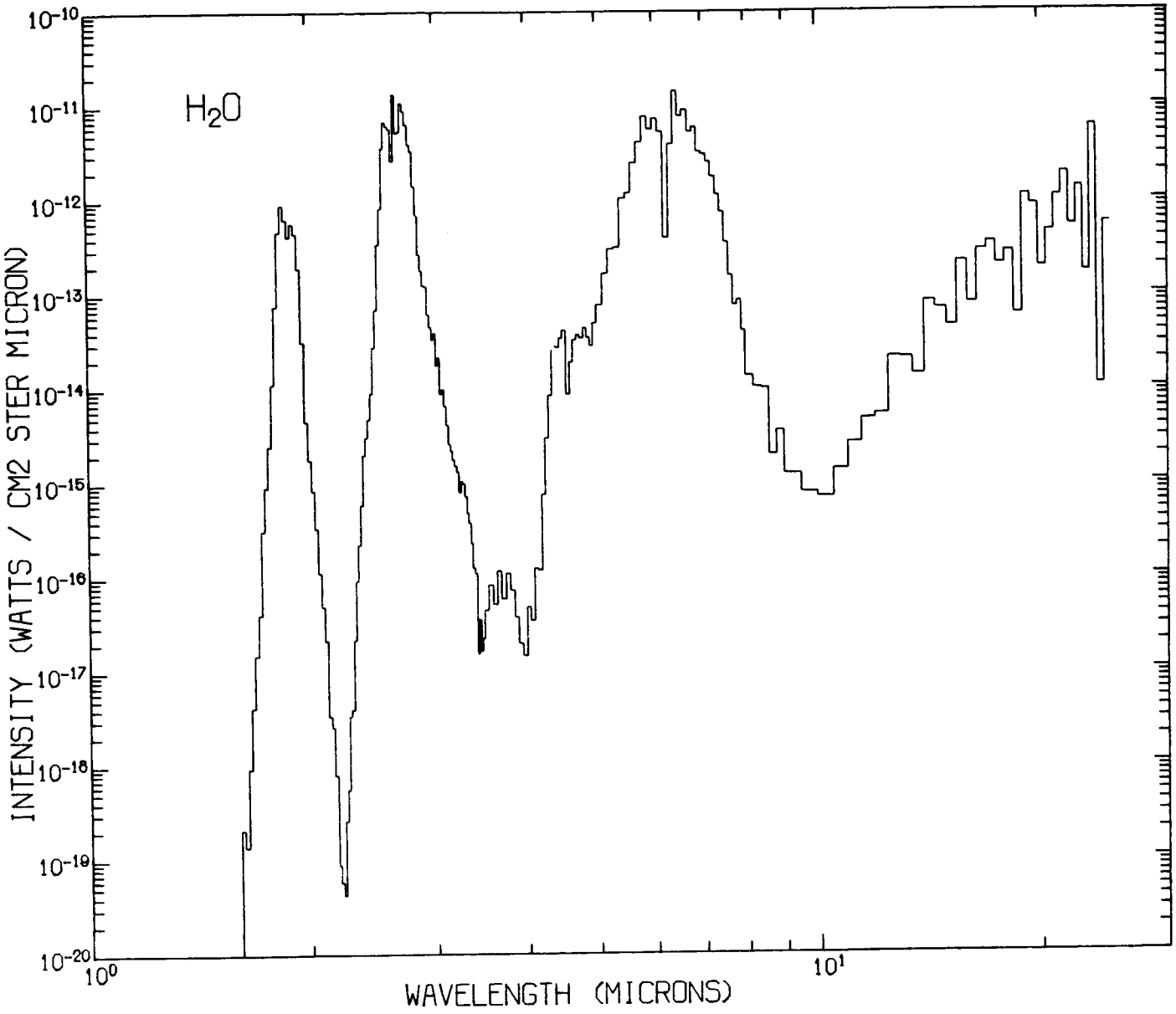

FIGURE 1 The intensity spectrum of 10^{12} molecules/cm^2 of H_2O is plotted from 1.6 to 25 μm. The molecules had an initial excitation temperature of 296K, but the energy level populations decay or are excited by the radiation from the earth and sun as the molecules move away from the Shuttle.

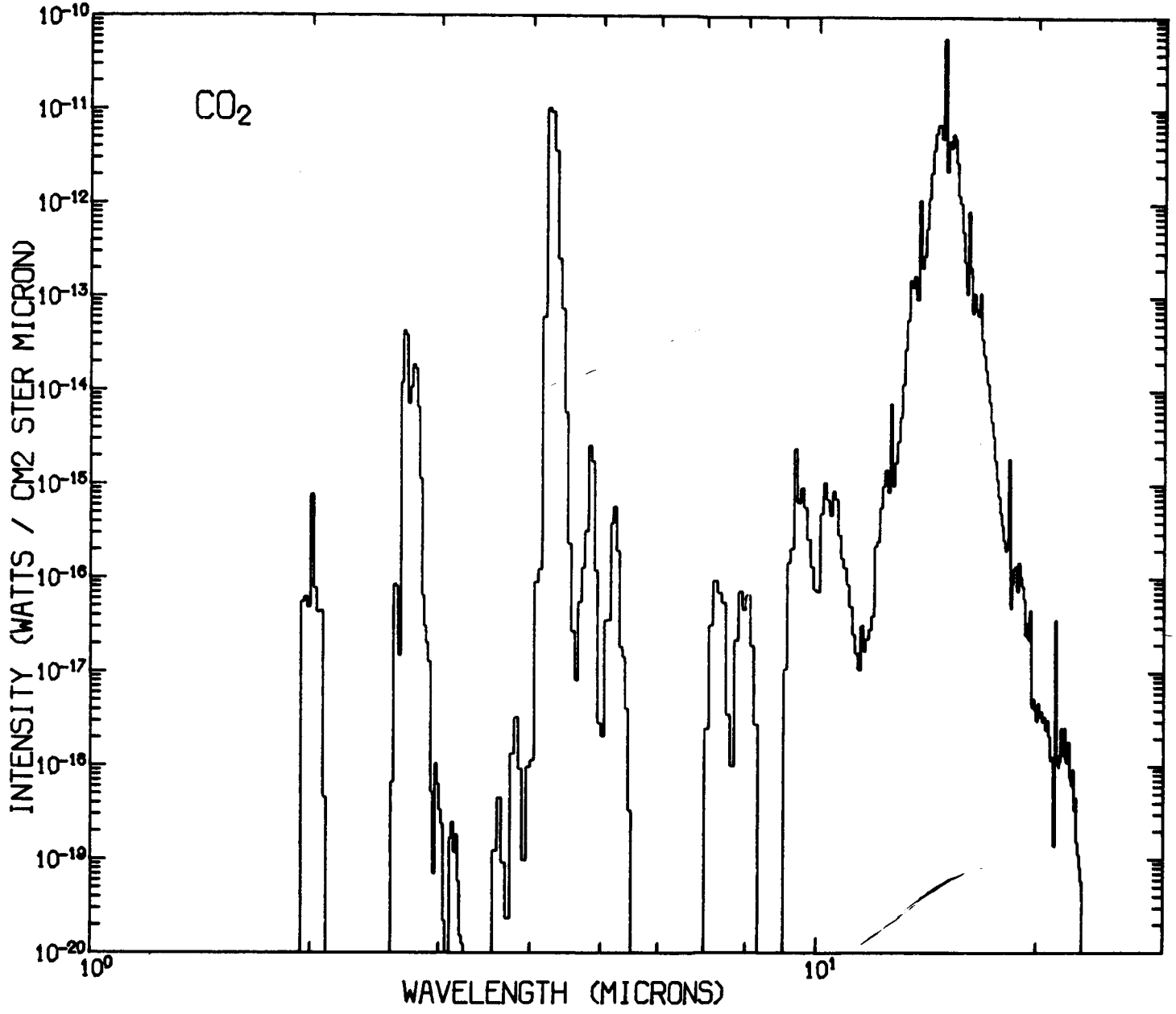

FIGURE 2 The intensity spectrum of 10^{11} molecules/cm^2 of CO_2 is plotted from 1.9 μm to infinity. The CO_2 molecules have the same excitation conditions as the H_2O in Figure 1.

achievable on the Space Shuttle, as discussed above. The spectra are somewhat different from those calculated previously for pure $^{1}H_{2}{}^{16}O$ and $^{12}C^{16}O_{2}$ with only radiative excitation from the ground state considered. For H_2O, the region at 4.5 μm is excited through fluorescence, and the minimum at 3.7 μm is partially filled in by HDO. $^{12}C^{16}O^{18}O$ adds extra bands in the 7-μm region.

The H_2O and CO_2 molecules are also excited by collisions with the ambient atmosphere. Because the mean free path through the atmosphere is so long (∿ kilometers), most molecules do not collide until they have already radiated down to the ground state. They are seen at all only because the probability of excitation is very large, due to the 7.7 km/sec velocity difference. Consequently, we can discuss the collisional excitation separately from the radiative excitation and add the two components of the spectrum together only at the very end. We chose an altitude of 350 km for the calculation; the average density at that altitude is 9.1×10^{-15} g/cm^3.[9] The atmosphere is predominantly atomic oxygen at this altitude. The average number density of oxygen atoms is 3.1×10^{8} atoms/cm^3. Since the intensity in the spectrum scales approximately as the density of the colliding oxygen atoms, the results can be scaled for other altitudes or nonaverage conditions.

An expression for the intensity of the radiation from collisionally excited molecules was derived by Simpson and Witteborn.[1] We rewrite it as

$$I = \frac{W}{\pi R^2 \Omega_{fov}} = \frac{h\nu}{4\pi} \frac{A}{v_{CM}} \frac{EP}{4\pi} \left\langle \frac{1}{d} \right\rangle \frac{N}{N_*} \qquad (1)$$

where W is the power on a detector from one line, R is the radius of the telescope, Ω_{fov} is the solid angle of the field of view, A is the transition probability for the line, h is Planck's constant, ν is the frequency, v_{CM} is the velocity of the center of mass of the colliding oxygen atom and the emitted H_2O or CO_2 molecule, E is the emission rate of the molecules over the whole Shuttle, P is the excitation probability, $\langle\frac{1}{d}\rangle^{-1}$ is the weighted average distance of the molecule when it radiates into the field of view, and $\frac{N}{N_*}$ is the fraction of the excited molecules that still have not decayed when they pass through the field of view. $\langle\frac{1}{d}\rangle$ and $\frac{N}{N_*}$ are integrals over the velocity distribution of functions that depend on the hard sphere cross section, the atmospheric density, and the transition probability. The cross sections for collisional excitation of H_2O by O and CO_2 by N_2 have been measured only at much lower energies, and for the 010 and 001 fundamentals only. We extrapolated the excitation of the 010 band of H_2O by oxygen (6.3 μm) measured by Dunn et al.[10] Rieger et al.[11] extrapolated the excitation of the 001 bands of H_2O (2.7 μm) and CO_2 (4.3 μm) by oxygen, using theoretical considerations that the cross section for excitation of CO_2 by O should be much larger than that for excitation by N_2. Elgin and Kolb[12] did the same for the 010 band of CO_2 (15 μm). Kolb et al.[13] and Kolb and Elgin[14] have calculated the pure rotational excitation of H_2O after collision with oxygen atoms. The earlier paper gives better agreement with experiment. No calculations are available for the rotational levels of an excited vibrational state, but Elgin and Kolb[12] suggest that 5% of the

center of mass energy goes into rotational excitation for CO_2. We used the same expression for H_2O. Although ad hoc, this does demonstrate that the bands will be greatly broadened, as though excited to a much higher temperature.

Because of the large uncertainties, we have calculated the collisionally excited spectrum at a much lower resolution than the radiatively excited spectrum. The results are given in Fig. 3 for E = $2x10^{20}$ molecules/sec of H_2O and in Fig. 4 for E = $5x10^{18}$ molecules/sec of CO_2. These emission rates correspond to column densities of $\sim 10^{12}$ molecules/cm^2 of H_2O and $\sim 10^{11}$ molecules/cm^2 of CO_2, with the emission plume geometry used by Rantanen and Ress.[2] Since the CO_2 comes from cabin leakage out the single walled bulkhead between the cabin and bay, a lower relative emission rate can produce the same column density looking straight out the bay than for outgassed H_2O. However, the expression for collisionally excited intensity was derived with the assumption that E/2 molecules/sec are emitted in the forward direction; therefore changing the Shuttle attitude will change the effective $E(CO_2)$ and hence $I(CO_2)$.

3. PARTICULATE CONTAMINANTS

A general discussion of spacecraft contaminant particles, their trajectories near the Orbiter and their infrared radiation is given by Simpson and Witteborn.[1] Particulate sightings from previous spacecraft have usually been associated with formation of ice particles near water vents or particle ejection associated with leaks or deliberate venting. The Orbiter is supposed to vent its fuel cell water in molecular form

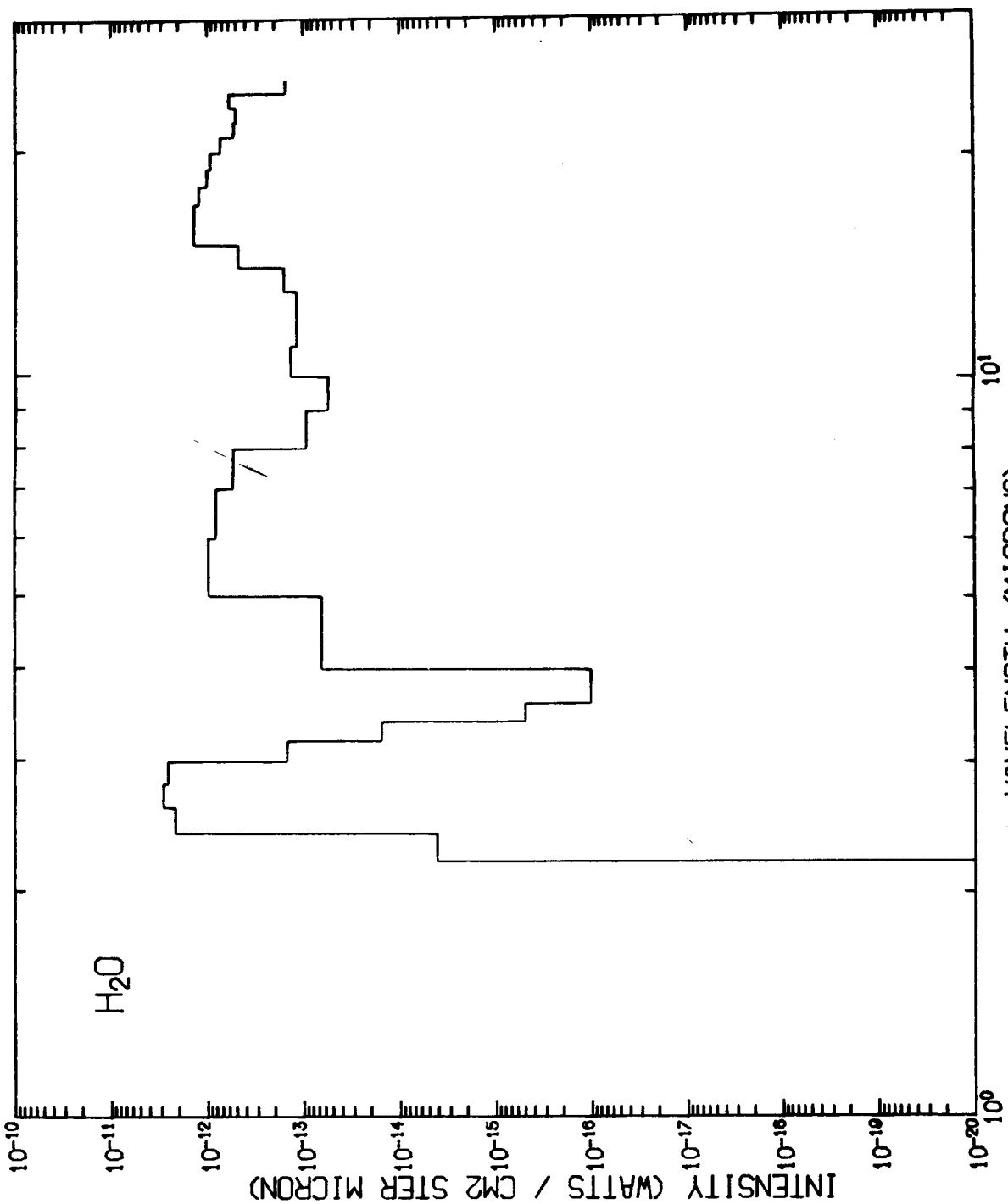

FIGURE 3 The intensity of the 2.7-μm and 6.3-μm fundamentals and pure rotation lines out to 25 μm is plotted for collisionally excited H_2O. The average atmospheric density for 350 km altitude was assumed. The emission rate of molecules from the Shuttle

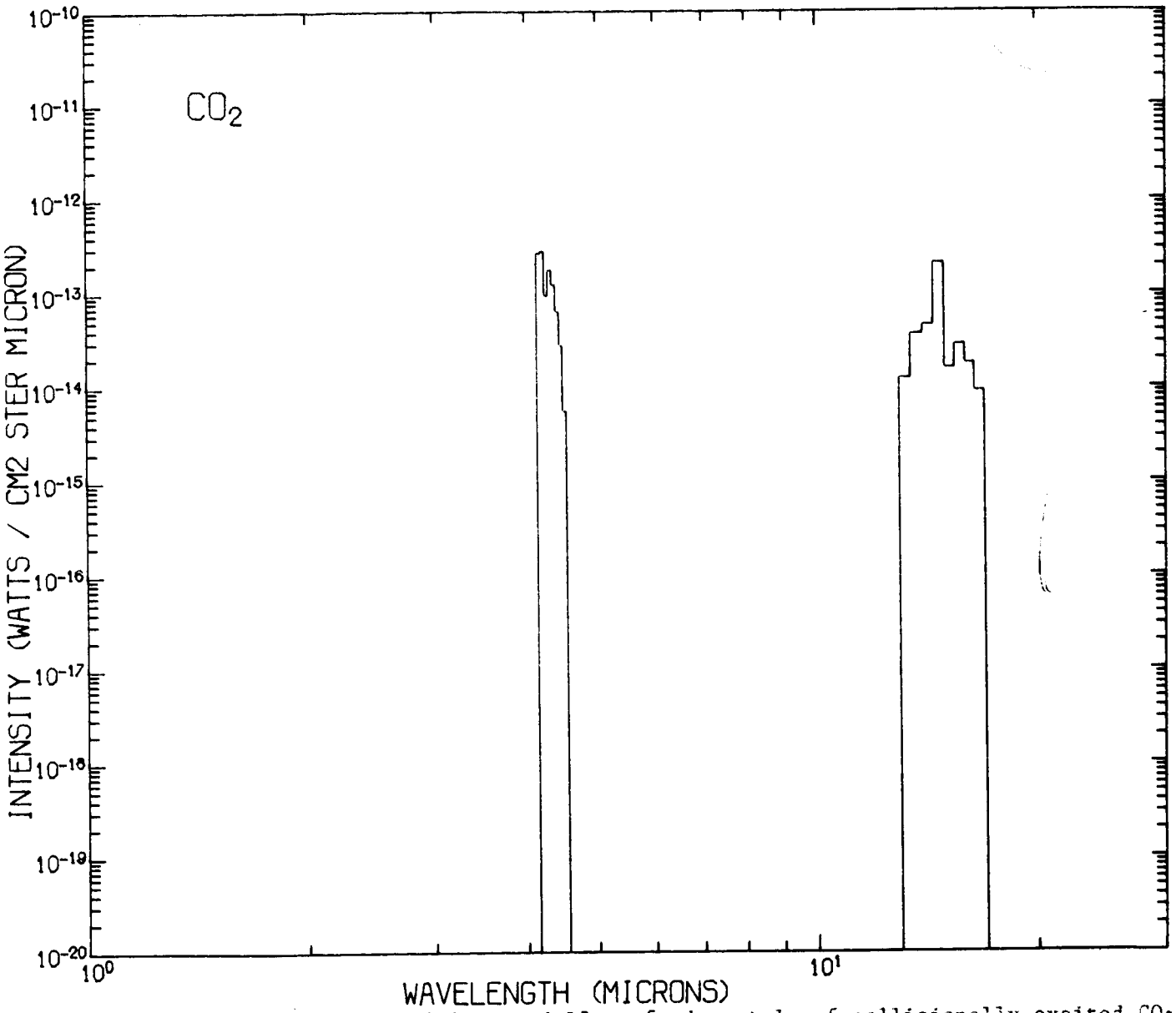

FIGURE 4 The intensity of the 4.3-μm and 15-μm fundamentals of collisionally excited CO_2 is plotted. (CO_2 has no pure rotation lines.) The average atmospheric density for 350 km altitude was assumed. The emission rate of CO_2 molecules used is based on the design specification limit of the leakage rate for the Shuttle cabin.

except when rapid venting is chosen. Other vents are manually controlled so that particulate sightings resulting from them could be limited to convenient times. Particles will be formed also from ejection of unburned fuel during vernier thruster firings. It is expected that observations sensitive to particle sightings will be made in the free-drift mode in which vernier thruster firings are suppressed for extended periods from 10 to 90 min depending upon attitude.[15] Particulate sighting rates resulting from anticipated cabin leaks are expected to be small. The seriousness of other particle sources such as paint flakes, abrasion products from moving parts, and loose dirt is difficult to evaluate because of poorly understood release mechanisms. In the past these sources have been adequately controlled by careful design and cleaning procedures. One release mechanism has been suggested that is not associated with any of the sources discussed above. This is the spallation of the Orbiter's surface by micrometeoroid impact. The ceramic tiles covering the Space Shuttle are coated with a thin layer of borosilicate glass to make them waterproof. When micrometeoroids hit the Shuttle they will be traveling at hypersonic velocities; microcraters will be formed in the glass coating and the spalled ejecta emitted at high velocities. Barengoltz[4] predicted the number of particles ejected per day; the number is substantial and of serious concern to a sensitive infrared telescope.

Hypervelocity craters have been investigated for many types of materials. They are especially of interest for studies of micrometeoroid

craters on lunar rocks. In these studies particles of ~1 μm in size are accelerated to 5 to 15 km/sec velocity and shot at different target materials. Vedder and his coworkers in particular have used glass targets. They then make electron micrographs of each resulting crater. An example is shown in Fig. 5. We are probably concerned with larger micrometeoroids at higher velocities and hence larger craters, but the features should be similar. The craters consist of a deep central pit with a splash rim of melted glass. The glass particles from the pit probably all reached high enough temperatures to melt; the area around some of the craters includes submicron size droplets of melted glass. We will assume that some of the smallest particles were still molten when ejected from the central pit of the crater. Goldstein[16] gave temperatures of 1400-1800K for the melting temperature of the borosilicate glass coating.

When the impacting particle has a higher velocity, the crater rim is also spalled off along with other chips of glass from around the outside of the rim. All this material has been shocked by the hypervelocity impact. Gault and Heitowit[17] estimated that about half of the kinetic energy (KE) of the micrometeoroid goes into kinetic energy of the ejecta and about 0.2 goes to increasing the internal energy of the shocked mass. Thus if we let the mass of ejecta $M_e = \alpha \frac{\rho}{S} KE$ where $\alpha \sim 0.5$ and S is the yield strength of the material[4] and $\Delta E = \beta\ KE = M_e\ C\ \Delta T$ where $\beta \sim 0.2$ and C is the specific heat, we find $\Delta T \sim 80K$. However Mandeville and Vedder[18] found a smaller mass of the ejecta which leads to $\Delta T = 200\text{-}350K$ for $\beta \sim 0.2$. This is an average temperature. The

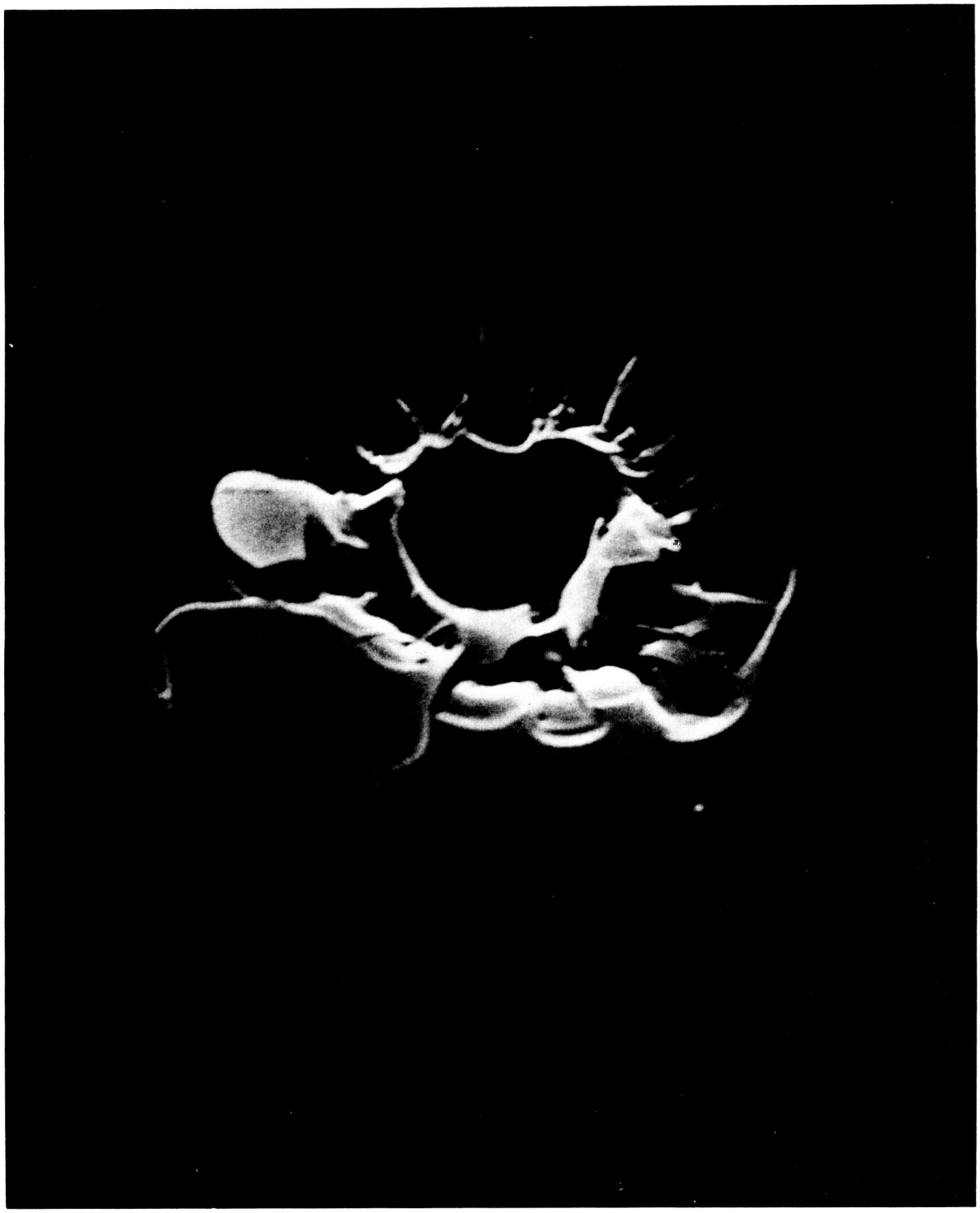

FIGURE 5 An electron micrograph of a crater on SiO_2 glass is shown. The impacting SiO_2 particle had a diameter of 3 μm and a velocity of 4 km/sec. The line going through the crater has a total length of 16μm.

temperature increase for the chips of glass from the rim could be lower if ejecta from the pit are hotter. With these uncertainties, we arbitrarily chose to plot spectra for $\Delta T = 150K$, or $T = 450K$ if a starting temperature of 300K was chosen. The final equilibrium temperature is also close to 300K.

To calculate the spectra of the particles we first assume that all particles are spherical. The diameters chosen ranged from 1 to 20 μm. We used the complete Mie theory for scattering and absorption by spheres. The equations are found in many books, such as van de Hulst[19] and Wickramasinghe.[20] The input parameters to a Mie scattering calculation are the size parameter x (the ratio of the particle circumference to the wavelength), the complex index of refraction $m = n - ik$, and the array of scattering angles. The output is the extinction efficiency $Q_{ext}(=\sigma_{ext}/\pi a^2$, where σ_{ext} is the extinction cross section and a is the particle radius), $Q_{sca}(=\sigma_{sca}/\pi a^2)$, and the angular dependencies. The emissivity ϵ equals the absorption efficiency $Q_{abs} = Q_{ext} - Q_{sca}$. The scattering and absorption properties of a particle with x near unity are very curious because the particle can influence much more of the incoming wavefront than its geometrical size. There can be very sharp fluctuations due to resonances (particularly if $k << 1$) and Q_{sca} and even Q_{abs} can be much larger than 1. That is, the particle can emit <u>more</u> than a blackbody at wavelengths where $Q_{abs} > 1$. These effects can be seen in the image brightness plots discussed below.

The next problem is the choice of the complex index of refraction m. In the infrared, m has been measured for similar materials (i.e.,

silicates) such as quartz and terrestrial and lunar rocks. Pollack et al.[21] have measured m for terrestrial obsidian, basalt, basaltic glass, and andesite. Since the optical constants n and k for basaltic glass generally fall in between the other materials, we used it for our first sample material for calculations of spectra between 2 μm and 50 μm. Beyond 50 μm, constants for fused quartz as given by Randall and Rawcliffe[22] were used.

The emissivities of the spalled particles were calculated from λ = 2 μm to 200 μm. The image of a nearby particle in the field of view will be out of focus; the size of the image is given by D/d where D is the diameter of the telescope and d is the distance to the particle. Then the power on a detector is given by $W_\lambda = \varepsilon\pi a^2 B_\lambda \Omega$, excluding the losses of a less than perfectly efficient system. We define the image brightness to be $I'_\lambda = W_\lambda/\Omega$, where Ω is the solid angle of the field of view ($\Omega = \pi\beta^2/4$ where β is the diameter of the field of view). Note that W_λ and I'_λ have no dependence on the diameter of the telescope so long as the particle is closer than $d = D/\beta$ (for a 1 m telescope with β = 1 arcmin, $d \leq 3.44$ km but for a 15 cm telescope with a one degree fov, $d \leq 8.7$ m). For distances greater than $d = D/\beta$,

$$W_\lambda = \frac{\pi^2 D^2}{4} B_\lambda \frac{a^2}{d^2} \qquad (2)$$

We have plotted the image brightness for 4 particle sizes in Fig. 6 for temperatures of 300K, 450K, and 1400K. A 300K blackbody is included for comparison. It is interesting to see that the famous 10-μm and 20-μm

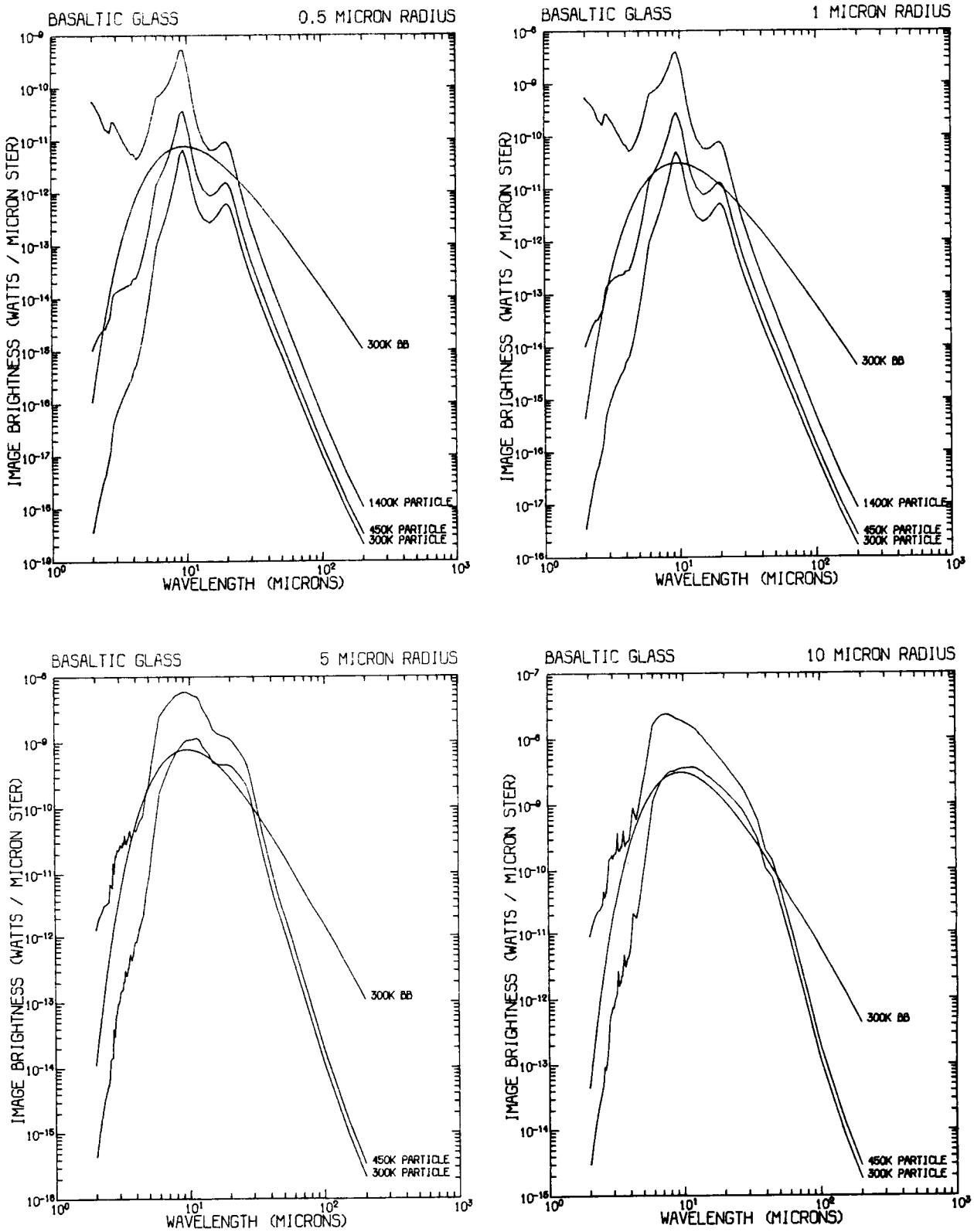

FIGURE 6 The image brightnesses for four sizes of particles of basaltic glass are plotted versus wavelength. The particles have temperatures of 300K, 450K, and 1400K. A 300K blackbody is plotted for comparison.

silicate features do not show up in the spectra of the larger particles. These particles are optically thick at intermediate wavelengths.

It should be possible to measure m for the ceramic tile coating. Goldstein[16] has provided transmission and reflection spectra of the black Shuttle coating, from which one can estimate n and k using dispersion theory.[21] However, the Shuttle coating is not uniform on a scale of a few microns, and it is not at all clear that particles a few microns in diameter would have the same properties as a large tile. To be specific, there are two types of coating, white and black. The white consists of small particles of glass sintered together and contains air bubbles 8 to 10 μm in diameter. The white color is due to scattering by the bubbles. To decrease the albedo of the white coating, 8 to 10 μm particles of silicon carbide have been added. The black coating has a very low albedo due to suspended particles of tetraboron silicide of size 1 to 10 μm.[16] In spite of these caveats, we used the dispersion analysis of Pollack et al. to get rough values for n and k from 7 to 25 μm. Spectra were then computed from 7 to 25 μm for particles with 2-μm radius. The spectra are generally similar to that of basaltic glass; the main features are the 10-μm and 20-μm silicate features and effects due to size.

The temperature of the particles must also be known in order to determine how much they radiate. When emitted, the particles are hot, but they radiate as $\bar{\epsilon}\,\sigma\,T^4$ and cool off with time. We will assume that the particles are also heated by the sun and earth. The brightness temperature of the earth varies greatly with wavelength and the season

of the subearth point, ranging from ~216K in the depths of the H_2O and CO_2 bands where the atmosphere is optically thick to >300K at visible wavelengths over a hot desert. Since the particles have their largest Q_{abs} around 10 and 20 μm where the atmosphere is relatively optically thin, we will choose a relatively hot earth, $T_\oplus = 280K$. Then the energy equation is

$$\frac{dE}{dt} = \frac{4}{3}\pi r^3 \rho C \frac{dT}{dt} = -4\pi r^2 \bar{\epsilon} \sigma T^4 + \alpha_{vis}\, \pi r^2 \Omega_\odot \frac{\sigma}{\pi} T_\odot^4 + \alpha_{IR}\, \pi r^2\, 2\pi \frac{\sigma}{\pi} T_\oplus^4 \quad (3)$$

where $C = 0.3$ calories/g °C and $\rho = 2.4$ g/cm^3 and $\Omega_\odot \frac{\sigma}{\pi} T_\odot^4 = 1.360 \times 10^6$ erg/cm^{2}sec. α is the absorbtivity. $\bar{\epsilon}$ is the temperature weighted emissivity $\bar{\epsilon} = \int_0^\infty \epsilon_\lambda B_\lambda \, d\lambda / \int_0^\infty B_\lambda \, d\lambda$. The spectra for basaltic glass were computed using values of $\bar{\epsilon}$ calculated for different particle sizes and temperatures. Linear interpolation was used to obtain intermediate values. We assumed $\alpha_{IR} = \bar{\epsilon}$ (280K). For α_{vis} we do not have a good value. Goldstein[16] gave $\alpha_{vis} = 0.3$ for the white Shuttle coating and $\alpha_{vis} = 0.9$ for the black. However these are bulk properties and include the bubbles and the silicon carbide or tetraboron silicide. That is, the material is effectively homogeneous. However the small spallation particles may or may not include the impurities, which are the main determinant of α_{vis}. Pure glass is much more transparent in the visible and, depending on particle size, can have α_{vis} very close to zero. Assuming that $\alpha_{vis} = 0.3$ or 0.9, we calculated $T(t)$ from the above equation for $T(t = 0) = 450K$. The particles cool very rapidly but more slowly for larger particles. The larger particles eventually come to a

lower temperature because of their larger values of $\bar{\epsilon}$. However, at 0.1 sec, which is when most of the particles in Barengoltz's model pass in front of a telescope, the particles are near their original temperatures. The temperature as a function of time for $T(t = 0) = 450K$ and $\alpha_{vis} = 0.3$ is given in Fig. 7. We have ignored the solid angle of the Shuttle itself in the above calculation. Since the Shuttle is slightly warmer than the earth, the effect of the solid angle of the Shuttle is that the particles will cool more slowly. The length of time that this effect is important depends on the velocity of the particles. Particles with $v \lesssim 10$ m/sec are still close to the Shuttle at t = 1 sec (these are the larger particles which cool more slowly anyway), but particles with $v \gtrsim 10^3$ m/sec (the smaller particles) have already moved sufficiently far away by t = 0.1 sec to no longer feel any effect. All particles have moved far enough away after a few seconds that the final particle temperatures are as shown in Fig. 7.

We can also make predictions of the particle sighting rates due to spallation of the Shuttle tiles by micrometeoroids. (Other particle sources, such as dust and ices, are far less predictable.) The number of particles produced per day from the Shuttle by spallation were predicted by Barengoltz.[4] We will use his distribution function for velocity and particle size, which are ad hoc and need to be measured, but will scale the mass of the particles produced to agree with the measurements of the mass ejected from glass bombarded by hypervelocity particles by Mandeville and Vedder.[18] For particles with $E < 1$ μJ, Mandeville and

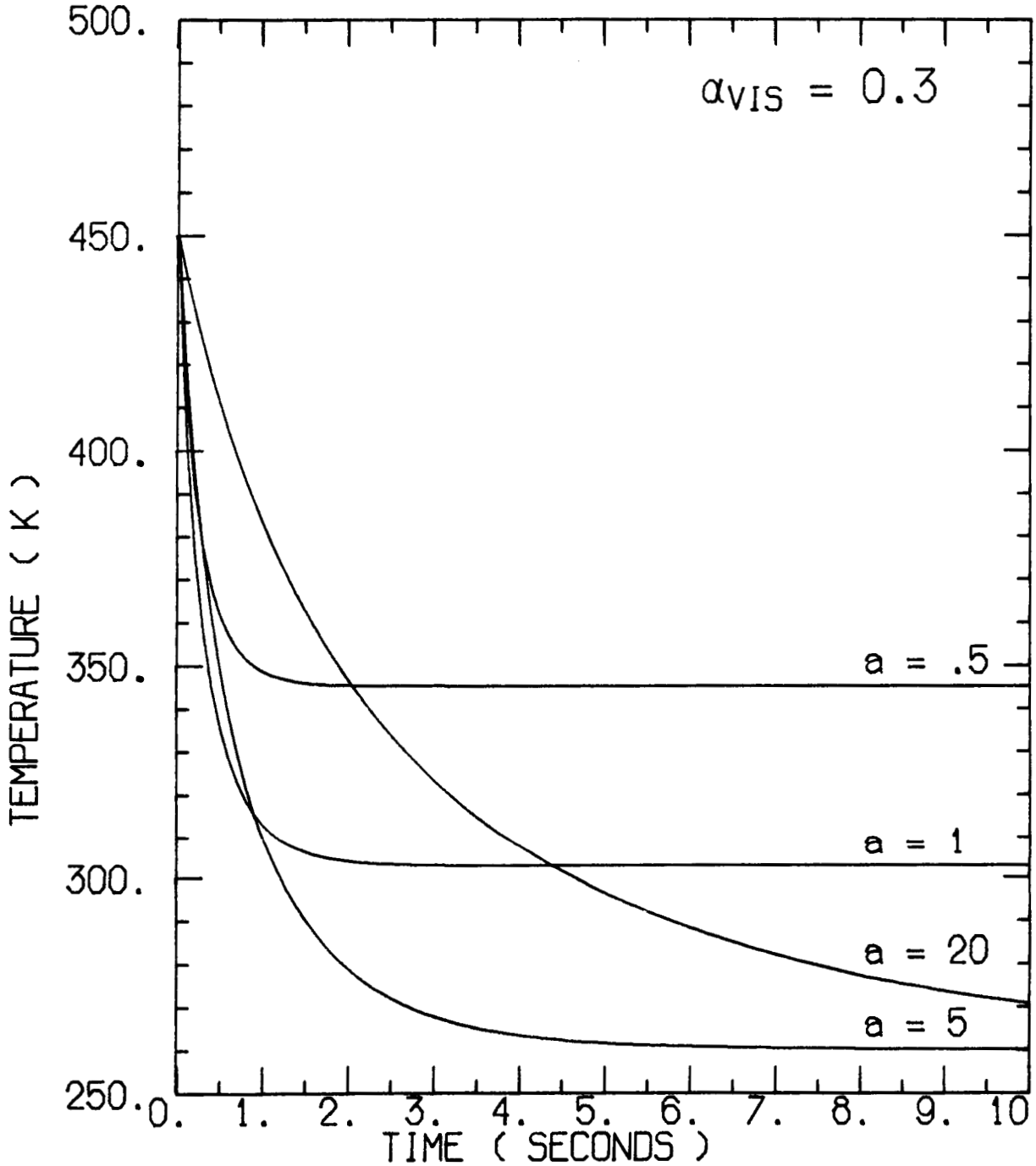

FIGURE 7 Particle temperatures as a function of time are plotted for particles with different radius a. The efficiency for visual absorption α equals 0.3.

Vedder found that $M_E = 230\ E^{1.1}$, where M_E is the mass of the ejecta from a single hypervelocity impact in picograms, and E is the kinetic energy of the impacting particle in μJ. Barengoltz's formula in these units is $M_E = 4000\ E$.[4] The energies of the micrometeoroids under consideration range from 4 to 10^4 μJ. Thus we must extrapolate Mandeville and Vedder's expression to much higher energies. Fortunately the difference in energy dependence from the theoretical is small, and the correction factors vary by only a factor of 2 over the whole range of energies. A second correction factor is for the flux of micrometeoroids near the earth. Barengoltz[4] used the Meteoroid Environment Model-1970;[23] whereas we will use the summary of Gault et al.[24] The latter has the same total mass flux as the former, but the numbers of very small micrometeoroids are much larger. The tiles on the surface of the Shuttle consist of a low density porous glassy foam coated with a thin dense layer of borosilicate glass. Barengoltz assumed that the smaller micrometeoroids would make microcraters in the glass coating (much like the craters studied by Vedder and his coworkers), but that the meteoroids with mass $\geq 10^{-6}$ g would break through the coating and embed themselves in the foam without releasing the large numbers of particles corresponding to the larger mass. Barengoltz (and we) ignored these larger particles; about one such particle per hour will hit the Shuttle. The final correction is that we used a different value for the total area of the Shuttle tiles. The result of all these corrections is that our number of total hits per day is a factor of ten smaller than that used by Barengoltz.[4] (He corrects his area to our value at the end of his paper.)

To calculate the fraction of particles that pass through the field of view, we first had to make several assumptions about the geometry of the situation. We assumed that particles are emitted randomly over the entire surface, then are swept back by the atmosphere and go into orbit around the earth. We assumed the atmosphere has the average density for 350 km altitude. The ejected particles can be divided into 2 classes depending on when they are sighted: 1) those that pass in front of the telescope immediately before atmospheric or orbital effects change the initial straight line trajectory, and 2) those that pass in front much later. For case 1, the important parameters are the diameter of the telescope and the distance it projects from the skin of the Shuttle. Of all particles emitted from the Shuttle, 0.2% fall into case 1 for a one m telescope projecting 3 m beyond the Shuttle. If the initial velocity of ejection is larger than a few m/sec, all the particles that pass in front of the telescope in case 2 are so far away that their out of focus images are smaller than the field of view. The fraction in this case is 0.5 x the field of view $\div 2\pi$. Thus, for a 15 arcmin fov the total fraction that passes through the field of view is 0.0026; for a 1 arcmin fov the fraction is 0.002.

We have run Monte Carlo calculations to determine the average energy deposited by a particle in the field of view as a function of particle size and initial velocity. These average brightnesses were then integrated over Barengoltz's size and velocity distributions to determine the fraction of particles in each brightness decade. These fractions,

the number of sightings per day, and the time interval between sightings are all given in Table 1. We have assumed that each detector has a 1 arcmin fov, but that there is a 15x15 array of detectors. The brightness given is that seen by any one detector, but the sighting could be on any part of the array. For all but the last entry it was assumed that the particles radiate like 300K blackbodies. However, some of the very smallest particles will be melted glass from the centers of the craters and will be much hotter. The last entry gives particles that would be too small to detect at 200K, but would be detectable if they were much

Table 1. Particle sighting rates for a 1 m telescope with a 1 arcmin fov (in spectral band near 10 μm).

Fraction that put < 10^{-17} Joules/10 μm on detector	.97
Number of sightings per day	$2x10^{4}$
Time between sightings	2 sec
Fraction with 10^{-16} > Joules/10 μm > 10^{-17}	$2x10^{-2}$
Number of sightings per day	$8x10^{2}$
Time between sightings	2 min
Fraction with 10^{-15} > Joules/10 μm > 10^{-16}	$4x10^{-3}$
Number of sightings per day	$1x10^{2}$
Time between sightings	10 min
Fraction with 10^{-14} > Joules/10 μm > 10^{-15}	$6x10^{-4}$
Number of sightings per day	$2x10^{1}$
Time between sightings	1 hr
Fraction with > 10^{-14} Joules/10 μm	$4x10^{-5}$
Number of sightings per day	$1x10^{0}$
Time between sightings	1 day
Fraction of additional small hot particles	$2x10^{-2}$
Number of sightings per day	$5x10^{2}$
Time between sightings	2 min

warmer and were seen within the first fraction of a sec after being emitted. All integration times are one sec. However, most of the very fast particles pass through the field of view in 0.1 sec or 0.01 sec or even less. The spectral bandwidth is 5 to 15 μm in all cases.

4. CONCLUDING REMARKS

The total background intensity expected from H_2O and CO_2 in the constrained (no thruster firings, liquid vents off, 40 h or more in space) Orbiter environment at 350 km is given by the sum of the intensities in Figs. 1, 2, 3 and 4. This total is less than 2×10^{-11} W $cm^{-2} ster^{-1} \mu m^{-1}$ throughout the 2 to 20 μm range except for a narrow peak several times higher at 15 μm. A cryogenically cooled telescope like SIRTF, having a one m unobscured aperture with a one arcmin diameter field of view, would see a background spectral flux of about 1×10^{-14} W μm^{-1} or less in this range. Examples of background and random noise under the above conditions are summarized for three cases in Table 2.

The field of view and bandwidth chosen in these examples are both near the largest expected for a single detector in astronomical

Table 2. Backgrounds due to contamination

Band (μm)	Power (W)	Photons (sec^{-1})	Noise from photon fluctuations (W $Hz^{-1/2}$)
2.1-3.1	1.7×10^{-15}	2.2×10^{4}	1.1×10^{-17}
3.1-4.1	4.1×10^{-17}	6.4×10^{2}	1.6×10^{-18}
6.0-7.0	3.6×10^{-15}	1.2×10^{5}	1.1×10^{-17}

applications shortward of 20 μm. Yet the random noise from H_2O and CO_2 emission is less than that in state-of-art detectors. Thus, the infrared emission from the expected molecular contaminant atmosphere of the Orbiter is not expected to be a serious limitation on the use of a sensitive infrared telescope, provided that thruster firings and water ventings are inhibited.

The particle sighting rates and resultant energy received by a 1 m telescope in a 1 arcmin field of view and 10 μm band (centered near 10 μm) have been estimated for the spallation products formed by impacting micrometeoroids. This is the most copious source of particles anticipated for the Orbiter environment when the thrusters are not firing and when the water vents are closed. Most instruments that have been suggested for SIRTF[25] operate in much narrower bands than the 10 μm used in Table 1 or else at longer wavelengths where the intensity of radiation from particles is lower (Fig. 6). Such instruments would be affected at intervals comparable to or longer than the longest expected integration time (20 min). One instrument under consideration, a sensitive broadband photometer, would be affected by particle sightings more frequently and would have to incorporate discrimination devices or logic for rejecting transient signals. Thus the particle environment also appears to be satisfactory for infrared astronomy, provided appropriate safeguards are taken in the design of sensitive, broadband instruments. However, the particle production rate and velocity distribution are very poorly understood. More work is needed to predict sources of particulates, release mechanisms,

and velocity distributions. Continuing efforts are needed to identify contaminants from payload materials as these are specified. Further tests are needed on the flash evaporators for the Orbiter to see if they really do emit water in molecular form only, with no ice particles.

5. ACKNOWLEDGMENT

We thank J. Vedder for permission to publish his electron micrograph of the crater in the glass target.

6. REFERENCES

1. Simpson, J. P. and Witteborn, F. C., Effect of the shuttle contaminant environment on a sensitive infrared telescope, Appl. Optics, 16:2051-2073 (1977).

2. Rantanen, R. O. and Ress, E. B., Payload/Orbiter Contamination Control Assessment Support, MCR 75-13, Martin Marietta Aerospace, Denver (1975).

3. Witteborn, F. C. and Young, L. S., Spacelab infrared telescope facility (SIRTF), J. Spacecraft and Rockets, 13:667-674 (1976).

4. Barengoltz, J. B., An Estimate of Particulates in the Vicinity of a Space Shuttle Orbiter due to Meteoroid Impact, Jet Propulsion Laboratory Report 900-793 (1977).

5. Schuerman, D. W. and Weinberg, J. L., Preliminary Study of Contaminant Particulates Around Skylab, NASA CR-2759, Available from National Technical Information Service, Springfield, Virginia 22161 (Oct. 1976).

6. Bareiss, L. E., Rantanen, R. O., and Ress, E. B., Payload/Orbiter Contamination Control Requirement Study, MCR 74-93, Martin Marietta Aerospace, Denver (1974).

7. Smith, R. E. ed., Space and Planetary Environment Criteria Guidelines for Use in Space Vehicle Development 1971 Revision, NASA TMX-64627 (1971).

8. McClatchey, R. A., Benedict, W. S., Clough, S. A., Burch, D. E., Calfee, R. F., Fox, K., Rothman, L. S., and Garing, J. S., AFCRL Atmospheric Absorption Line Parameter Compilation, AFCRL-TR-73-0096, Bedford, Mass. (1973).

9. CIRA 1972, COSPAR International Reference Atmosphere 1972, Akademie-Verlag, Berlin (1972).

10. Dunn, M. G., Skinner, G. T., and Treanor, C. E., Infrared radiation from H_2O, CO_2, or NH_3 collisionally excited by N_2, O, or Ar, AIAA J. 13:803-812 (1975).

11. Rieger, T. J., Tait, K. S., and Baum, H. R., Atmospheric interaction radiation from high altitude rocket exhausts, J. Quant. Spectrosc. Radiat. Transfer, 15:1117-1124 (1975).

12. Elgin, J. B. and Kolb, C. E., Extensions of Plume Interference Prediction Capabilities, Final Technical Report, ARI RR-104, Aerodyne Research, Inc., Bedford, Mass. (1977).

13. Kolb, C. E., Baum, H. R., and Tait, K. S., Classical calculations of H_2O rotational excitation in energetic atom-molecule collisions, J. Chem. Phys., 57:3409-3416 (1972).

14. Kolb, C. E. and Elgin, J. B., Classical calculations of NH_3 and H_2O rotational excitation in energetic collisions with atomic oxygen, J. Chem. Phys., 66:119-124 (1977).

15. Rockwell International Corporation, Study to Analyze Integration of Shuttle Infrared Telescope Facility (SIRTF) and the Biomedical Experiments Satellite Facility (BESS) Into the Space Transportation System, Final Report, SD77-SR-0003, Vol. 1 (1977).

16. Goldstein, Howard (1977) private communication.

17. Gault, D. E. and Heitowit, E. D., The partition of energy for hypervelocity impact craters formed in rock, in Proc. Sixth Hypervelocity Impact Symposium, Vol. 2, pp. 419-456 (1963).

18. Mandeville, J. C. and Vedder, J. E., Microcraters formed in glass by projectiles of various densities, Earth and Planet. Sci. Lett., 11:297-306 (1971).

19. van de Hulst, H. C., Light Scattering by Small Particles, John Wiley & Sons, Inc., New York (1957).

20. Wickramasinghe, N. C., Interstellar Grains, Chapman and Hall Ltd., London (1967).

21. Pollack, J. B., Toon, O. B., and Khare, B. N., Optical properties of some terrestrial rocks and glasses, Icarus, 19:372-389 (1973).

22. Randall, C. M. and Rawcliffe, R. D., Refractive indices of germanium, silicon, and fused quartz in the far infrared, Appl. Optics, 6:1889-1895 (1967).

23. Meteoroid Environment Model 1970 (Interplanetary and Planetary), NASA SP-8038 (1970).

24. Gault, D. E., Horz, F., Brownlee, D. E., and Hartung, J. B., Mixing of the lunar regolith, Geochim. Cosmochim. Acta (Suppl 5), 5:2365-2386 (1974).

25. McCreight, C. R., Walker, R. G., and Witteborn, F. C., IRAS and SIRTF: Implications of scientific objectives on focal plane sensitivity requirements, paper 132-12 given at the Society of Photo-Optical Instrumentation Engineers (SPIE) Technical Symposium, Vol. 132. Utilization of Infrared Detectors (Jan. 1978).